

Interstitial and Interlayer Ion Diffusion Geometry Extraction in Graphitic Nanosphere Battery Materials

Attila Gyulassy, Aaron Knoll, *Member, IEEE*, Kah Chun Lau, Bei Wang, *Member, IEEE*, Peer-Timo Bremer, *Member, IEEE*, Michael E. Papka, Larry A. Curtiss, and Valerio Pascucci, *Member, IEEE*.

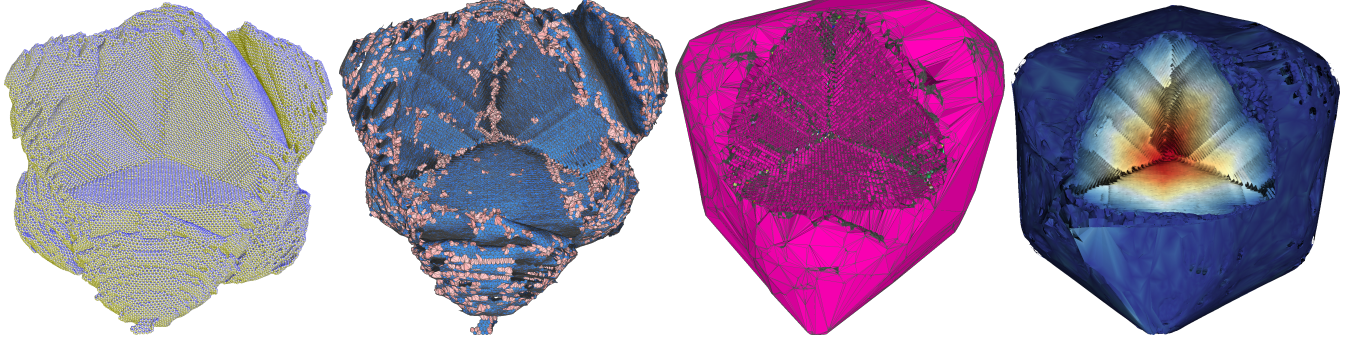


Fig. 1. A carbon nanosphere anode material is simulated with an annealing process using classical molecular dynamics (left). To understand the efficacy of this material in battery design, we seek to understand the adsorption of lithium. In graphitic carbon, lithium motion is governed by the arrangement of carbon rings: while 6-member rings block lithium diffusion through layers of graphene, higher valence rings permit it. Our approach turns to topological analysis of the distance function, constructing explicit triangulations to represent carbon rings, classifying them as blocking (blue) or non-blocking (pink) (middle left). We use our representation to quantify both the portions of the nanosphere that are accessible from the exterior (dark pink) (middle right), as well as studying the effects of defects on the diffusion distance needed to saturate the nanosphere (right).

Abstract— Large-scale molecular dynamics (MD) simulations are commonly used for simulating the synthesis and ion diffusion of battery materials. A good battery anode material is determined by its capacity to store ion or other diffusers. However, modeling of ion diffusion dynamics and transport properties at large length and long time scales would be impossible with current MD codes. To analyze the fundamental properties of these materials, therefore, we turn to geometric and topological analysis of their structure. In this paper, we apply a novel technique inspired by discrete Morse theory to the Delaunay triangulation of the simulated geometry of a thermally annealed carbon nanosphere. We utilize our computed structures to drive further geometric analysis to extract the interstitial diffusion structure as a single mesh. Our results provide a new approach to analyze the geometry of the simulated carbon nanosphere, and new insights into the role of carbon defect size and distribution in determining the charge capacity and charge dynamics of these carbon based battery materials.

Index Terms—materials science, morse-smale, topology, Delaunay, computational geometry

1 INTRODUCTION

Material science studies a wide range of phenomena at various scales, using different computational codes for different purposes. Molecular dynamics (MD) are the main computational technique to simulate chemical-physical systems in large spatio-temporal scale at the atomistic level. General computational studies must trade between computational cost and physical accuracy. At small spatio-temporal scales in Ångströms and femtoseconds, first-principles *ab initio* molecular dynamics (AIMD) codes, e.g., employing density functional theory, (DFT) can accurately simulate electronic structure and bonding en-

ergetics. For larger systems on the order of millions of atoms over nanoseconds, material scientists employ classical MD codes with approximate atomic potential or force-field. As the underlying structure and assumptions of simulations change, so too must techniques for visualizing and analyzing them.

Carbon nanospheres are promising anode materials for a new generation of lithium ion-based battery technologies. These novel structures can be synthesized through autogenic pressure reactions by the recycling of wasted plastic materials [47]. To optimize the design and synthesis of these novel carbon materials, one has to understand their basic structural properties and lithium storage capability at the fundamental atomistic level. To model this computationally, we have the choice of precise small-scale models (hundreds of atoms over femtoseconds using DFT) and less accurate large-scale models (thousands or millions of atoms over nanoseconds, using MD). DFT simulations produce electronic structure properties: the electronic wavefunction of the system, or all-electron density can be used in scalar-field analysis. In real world application, experimentally synthesized nanospheres would be on the order of 100 nm to 1 μm , consisting of hundreds of thousands to billions of carbon atoms. Classical MD must be used for phenomena at this scale, however the simulations produced with time-dependent atomic motion in trajectories produce neither the correct electronic structure properties nor a scalar field that is required for topological analysis.

Moreover, with both AIMD and classical MD methods we can sim-

- Attila Gyulassy, Aaron Knoll, Bei Wang, and Valerio Pascucci are with SCI Institute, University of Utah. E-mail: jediati knolla beiwang pascucci@sci.utah.edu.
- Kah Chun Lau, Michael E. Papka, and Larry A. Curtiss are with Materials Science Division, Argonne National Laboratory. E-mail: kclau papka curtiss @anl.gov.
- Peer-Timo Bremer is with Lawrence Livermore National Laboratory. E-mail: bremer5@llnl.gov.

Manuscript received 31 Mar. 2014; accepted 1 Aug. 2014; date of publication xx xxx 2014; date of current version xx xxx 2014.

For information on obtaining reprints of this article, please send e-mail to: tvcg@computer.org.

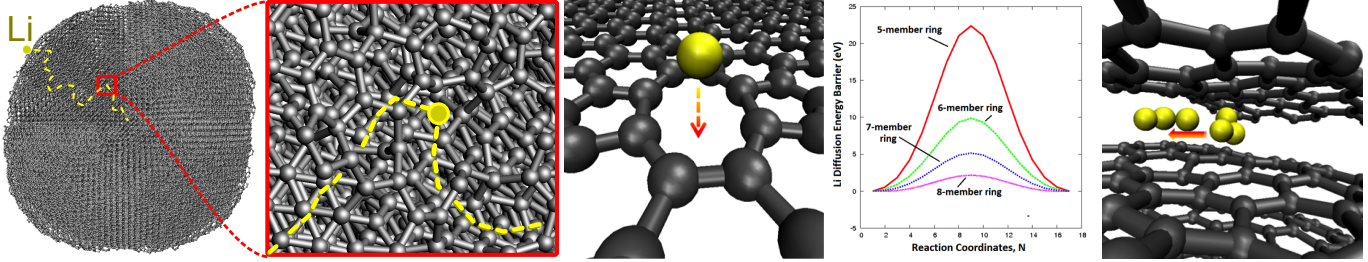


Fig. 2. *Left:* Where lithium (yellow) may diffuse in carbon (dark gray) nanosphere relates to its utility as a battery material. However, direct simulation requires prohibitively long time scales. Instead, the motion is computed for local configurations. *Center:* The energy barriers for *interlayer* lithium diffusion through the center of n-membered ring at a single graphene sheet are obtained from DFT calculation. Rings with valence six or less block lithium diffusion. *Right:* Interstitial 1D-, 2D-diffusion of lithium is principally limited by the dynamics of adjacent lithium ions distribution within the graphitic layers obtained from AIMD simulation, with no energy barrier from the carbon itself.

ulate thermal annealing of various-sized nanospheres, but we cannot accurately model the complex diffusion dynamics of lithium ions within these structures. While the physical properties of such systems (e.g. sp^2/sp^3 ratio of carbon bonds of the carbon structure) are generally understood, the long time scale of the ion diffusion and transport process (charging the battery) occurs over the course of microseconds or longer, which would be too costly and inaccurate to compute with current MD techniques. However, the basic diffusion characteristics of nanospheres can be understood via topological and geometric analysis of the local atomic structures. For DFT data, it is possible to use Morse-Smale decomposition of the wavefunction to determine the paths that diffusing ions may take [25]. This analysis sheds light on the interstitial and interlayer structure of the nanosphere, and provides metrics for assessing theoretical performance of the battery anode.

Topological analysis would be desirable for larger data from classical dynamics as well. However, we are faced with two challenges: classical MD data do not provide any “ground-truth” scalar field for us to conduct such analysis; and the size of these data make analysis of derived structured data costly. Although several techniques have been proposed to compute diffusion paths in molecular structures, the specific properties of lithium interacting with graphitic carbon prevent straightforward application of a known solution. In particular, in a molecule formed by deformed graphitic sheets, the diffusion of lithium is regulated by the local arrangement of carbon atoms in rings, not distance or charge density.

In this paper, we present a new approach to analyze lithium diffusion in graphitic carbon that considers the local arrangements of atoms. First computing a Delaunay triangulation of the raw atom geometry, the algorithm produces triangular patches that close the interior of loops of edges in the triangulation, thereby enabling classification of structures that permit or prevent lithium ion diffusion. Furthermore, we present visualizations that illuminate how lithium penetrates a nanosphere. In addition, we are able to quantify for the first time the effect of small-scale defects on adsorption capabilities. Significantly, our analysis of a large (30-Å diameter) nanosphere suggests increased importance of interlayer geometry and large fracture features in accumulating and storing lithium. Our work shows that topological analysis can be used to characterize larger structures from molecular dynamics, and suggests an alternative to direct large-scale AIMD or MD simulations.

2 BACKGROUND

We provide a brief overview of necessary background, including basic information on the simulation generating the carbon nanospheres and how lithium diffuses in these materials. Figure 2 provides an overview of the problem set-up: direct simulation of lithium motion in complex geometries is impractical due to the long time scales involved; instead, diffusion in the nanosphere is computed by finding simple configurations, for instance, rings of certain valence, or interstitial space. An overview of geometric and topological concepts used in our analysis approach are also provided.

2.1 Simulating Carbon Nanospheres

In designing more powerful and resilient Li-ion batteries (LIB), finding novel materials with robust cycling performance and high charge capacity are extremely important. Carbon graphites are among the most intensively studied anode materials due to their high coulombic efficiency and high electrochemical stability [51]. Numerous promising research directions have been proposed to increase gravimetric capacity of low dimensional carbon nanomaterials [38, 48, 39, 47]. The carbon nanospheres in this study were synthesized by high-temperature autogenic reactions of hydrocarbon precursors (e.g., polyethylene from plastic waste), enabling synthesis of battery anodes from daily recycled materials [47]. As discussed in Section 1, to simulate this spherical morphology of carbon at atomistic scales one must trade between scale and accuracy: small carbon nanospheres (hundreds of atoms) can be modeled based on density functional theory (DFT) or *ab initio* molecular dynamics (AIMD) codes such as VASP [32], whereas large (experimental-scale) nanospheres must employ more approximate classical molecular dynamics. The thermally annealed nanosphere in our example was simulated in LAMMPS [46], sculpted from a solid block of carbon in diamond bulk structures, heated to a high temperature (2500 Kelvin) via molecular dynamics, and then annealed to 300 degrees Kelvin. The resulting “nanosphere” possesses numerous channels that can accommodate lithium ion diffusing through both interstitial and interlayer defects in the local graphitic structures of carbon nanospheres [47]. While effective, statistical analysis cannot fully quantify the charge capacity of these structures: we wish to analyze the possible lithium diffusion paths that may diffuse or transport through the inside or outside of the carbon nanosphere.

Simulating ion diffusion in electrified heterogeneous electrode/electrolyte interfaces is a fundamental problem in the design of electrochemical energy conversion and storage devices such as batteries and fuel cells [27]. Accurate description of electronic properties of materials (e.g. bulks, surfaces, interfaces, phase changes, etc.), is generally limited by the approximate exchange-correlation functionals, and limited system size due to the poor computational scaling [10]. Classical molecular dynamics are limited by less accurate and non-transferrable atomic force fields. Even given unlimited compute time, straightforward simulation via classical MD will often result in incorrect thermodynamic equilibrium properties, and potential energy surfaces that do not accurately describe a complex system. Moreover, validation of an atomistic simulation with state-of-the-art *in situ* or *in operando* experimental observation of the electrochemical system is difficult. For theoretical modeling and simulation, direct computation of Li ions diffusion paths derived from “on-the-fly” trajectories at various anisotropic local environments at the atomistic level are too expensive for large spatio-temporal scale. With both current AIMD and classical MD methods, the simulation of various size of carbon morphologies (including nanospheres) at thermal equilibrium is possible, however the dynamics of such “rare events” at a long time scale are simply too expensive to compute.

Nonetheless, to understand lithium ion diffusion and storage in

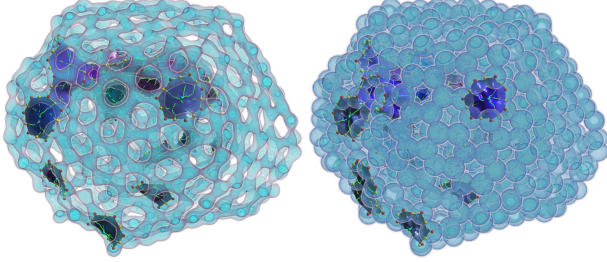


Fig. 3. Morse-Smale analysis of a 732-atom nanosphere, computed via DFT. *Left:* using the electronic wavefunction. A volume rendering is shown, with each blocking patch assigned a semi-random color. *Right:* using the distance field.. As shown in [25], the distance field can be used as a suitable, though not identical, substitute for the wavefunction.

carbon structures, we can conduct smaller DFT experiments studying dynamics and energetics of diffusion. Li diffusion paths in carbon nanospheres can be 1-, 2- or 3-dimensional, depending on the anisotropy of the local structure and the presence of defects, tunnels, surfaces active or inactive upon lithiation or delithiation during the electrochemical cycling. Binding energies, redox potentials, and hopping energy barriers, diffusion paths and ions dynamics can strongly deviated from the a graphite bulk values near surfaces or interfaces.

A Model for Lithium Motion. Given that directly simulating lithium diffusion in the nanosphere is computationally infeasible, we instead turn to models that describe its motion given local configurations of atoms. As shown in Figure 2, lithium diffusion in carbon nanospheres can be represented either as *interstitial* (lateral along or within graphene layers) or *interlayer* (through defects in the layers themselves). Small scale computations [47, 25] reveal that: (1) interstitial motion is governed only by the presence of other lithium atoms, and is otherwise free; and, (2) the energy required for interlayer diffusion depends on the number of atoms in a carbon ring. In particular, valence six and less rings block the diffusion of lithium, whereas valence seven or more rings permit interlayer diffusion. Thus, the key challenge in our work is to identify carbon rings, and count their valence, and study how their arrangements block or permit lithium motion.

For small DFT models, we can use the electronic wavefunctions of the system, e.g. the simulated electronic structure, as input for scalar-field topological analysis (specifically, Morse theory). With DFT data, one can assume one-to-one correspondence between carbon atoms, covalent bonds and components of the Morse-Smale complex of the scalar function. From this information, the carbon defects and possible void spaces that are present in the carbon nanospheres can be identified qualitatively [25]. Moreover, previous work has shown that a distance field approximation of the wavefunction yields similar diffusion paths, as illustrated in Figure 3. This is crucial for our analysis of larger molecular dynamics computations: without a wavefunction on which to conduct MS decomposition, we must induce the topology of the nanosphere from raw atom geometry and the distance field.

2.2 Geometry and Topology

We provide a brief overview of Delaunay triangulations, their dual, the Voronoi diagram, and relate them to the Morse complex of the distance function. Finally, we review discrete Morse theory from the perspective of simplicial collapse, as this intuition is utilized in our approach to computing diffusion geometry in the nanospheres.

Simplicial Complex. The algebraic topology concept of *simplicial complex* is typically used to represent a topological space. A k -dimensional simplex σ (a.k.a. a k -simplex) is the convex hull of $k+1$ affinity independent points. A *face* α of σ is any simplex that is the convex hull of a subset of the $k+1$ points in \mathbb{R}^d . We denote the face relation with $\alpha < \sigma$. If $\dim(\alpha) = \dim(\sigma) - 1$ we say α is a *facet* of σ and σ is a *co-facet* of α , and we denote this $\alpha \prec \sigma$. Typically, we call an 0-simplex a *vertex*, a 1-simplex an *edge*, a 2-simplex a *triangle* and a 3-simplex a *tetrahedron*. A *simplicial complex* K in \mathbb{R}^d is a collection of simplices in \mathbb{R}^d such that: (a) every face of a simplex of K is in K ; and (b) the intersection of any two simplices of K is a face of each of

them. A *subcomplex* L of K is a sub-collection of K that contains all faces of its elements. The *p-skeleton* of K is a subcomplex of K that contains all simplices in K of dimension at most p , denoted as K^p . Therefore K^0 contains the vertices of K , $K^1 \setminus K^0$ contains the edges of K , etc. $|K|$ denotes the subset of \mathbb{R}^d that is the union of simplices of K . See [40] for introductory materials.

Voronoi Diagram and Delaunay Triangulation. For a finite set of points $P \subseteq \mathbb{R}^d$, the *Voronoi cell* (or *Voronoi region*) of $p \in P$, denoted as V_p , is the set of points in \mathbb{R}^d whose (Euclidean) distance to p is no greater than any other points in P . The partitioning of \mathbb{R}^d into a collection of Voronoi cells of all points in P forms the *Voronoi diagram*. The *Delaunay triangulation* of P is the dual graph of its Voronoi diagram. These concepts could be extended to their corresponding weighted version by assigning a weight to all points $p \in P$ and modifying the definition of distance between a point in \mathbb{R}^d and a weighted point p .

Morse Complex. Let f be a real-valued smooth map $f : M \rightarrow \mathbb{R}$ defined over a compact d -manifold M . A point $p \in M$ is critical when $|\nabla f(p)| = 0$, i.e. the gradient is zero, and is non-degenerate when its Hessian (matrix of second partial derivatives) is non-singular. The function f is a *Morse function* if all its critical points are non-degenerate and no two critical points have the same function value. In this case the *Morse Lemma* states that there exists local coordinates around p such that f has the following *standard form*: $f_p = \pm x_1^2 \pm x_2^2 \cdots \pm x_d^2$. The number of minus signs in this equation gives the *index* of critical point p . In three-dimensional functions, minima are index-0, 1-saddles are index-1, 2-saddles are index-2, and maxima are index-3.

An integral line in f is a path in M whose tangent vector agrees with the gradient of f at each point along the path. The integral line passing through a point p is the solution to $\frac{\partial}{\partial t} L(t) = \nabla f(L(t))$, $\forall t \in \mathbb{R}$, with initial value $L(0) = p$. Each integral line has an origin and destination at critical points of f , at $t = \pm\infty$. *Ascending* and *descending* manifolds are obtained as clusters of integral lines having common origin and destination respectively. The descending manifolds of f form a cell complex that partitions M ; this partition is called the *Morse complex*. An index- i critical point has an i -dimensional descending manifold. The intersection of the ascending and descending manifolds produces a refinement of the two complexes, which we refer to as the *Morse-Smale complex*.

Our interest in Morse theory in this application is motivated by the relation of the distance function of a set of points to the Voronoi diagram and Delaunay triangulation. Each d -dimensional cell of a three-dimensional Voronoi diagram corresponds exactly to the ascending d -manifold of an index- $(3-d)$ critical point in the distance function. Furthermore, there is an injective map between index- i critical points of the distance function and i -simplices of the Delaunay triangulation. This is important, as all features of the distance function are guaranteed to be preserved as some simplex of a Delaunay triangulation.

Discrete Morse Theory. Although a complete overview of discrete Morse theory [22] is outside the scope of this paper, we use basic notions to simplify our discussion. In particular, we utilize *simple homotopy* extensions and collapses [11]. The *star* of a simplex α , denoted $St(\alpha)$, is the set of co-faces of α . The *link* of α is the closure of the star, minus the star itself, $Lk(\alpha) = \overline{St(\alpha)} - St(\alpha)$. Let K be a simplicial complex, the *centroid* $C : K \rightarrow M$ of an i -simplex $\alpha \in K$, $C(\alpha)$, is the average position of its vertices. A *vector* in the discrete sense is a pairing of cells $\langle \alpha^{(i)}, \beta^{(i+1)} \rangle$, where $\alpha \prec \beta$. We say that an arrow points from $\alpha^{(i)}$ to $\beta^{(i+1)}$. The *direction* of the arrow relates the combinatorial notion of the pairing to the geometric interpretation of flow, and is given by $C(\beta^{(i+1)}) - C(\alpha^{(i)})$. Intuitively, this vector simulates a direction of flow. A *discrete vector field* V on K is a collection of pairs $\langle \alpha_j^{(i)}, \beta_j^{(i+1)} \rangle$ of cells of K such that each cell is in at most one pair of V . All unpaired cells are *critical* cells. Given a discrete vector field V on K , a *V-path* is a sequence of cells

$$\alpha_0^{(i)}, \beta_0^{(i+1)}, \alpha_1^{(i)}, \beta_1^{(i+1)}, \alpha_2^{(i)}, \dots, \beta_r^{(i+1)}, \alpha_{r+1}^{(i)}$$

such that for each $j = 0, \dots, r$, the pair $\langle \alpha_j^{(i)}, \beta_j^{(i+1)} \rangle \in V$, and $\alpha_j^{(i)}$ and $\alpha_{j+1}^{(i)}$ are both facets of $\beta_j^{(i+1)}$. A discrete vector field in which each V -path has disjoint start and end-points is a *discrete gradient field*, denoted G , of a discrete Morse function. Note that this condition implies that a discrete gradient field G does not contain any loops.

The discrete gradient field G is the combinatorial analogue of ∇f , enabling the notions from continuous Morse theory to transfer to the discrete setting. *Discrete ascending and descending manifolds* are given by the collection of V -paths having the same critical cell as origin and destination, respectively. Similar to the continuous setting, the discrete ascending and descending manifolds form a partition of \mathbb{M} . In our approach we construct a subset of a complete discrete gradient field, such that the descending 2-manifold from every critical triangle is guaranteed to close the interior of loops of marked edges and vertices.

3 RELATED WORK

We review works that are most relevant to our proposed techniques, which are inspired by applying discrete Morse theory to Delaunay triangulations. We begin with a few bibliographic notes on Voronoi diagrams and Delaunay triangulations. Then we focus on geometric and topological methods for the detection of protein cavities (i.e. voids, pockets and tunnels) in molecular shape analysis, in particular, those that rely on the computation of Voronoi diagrams and Delaunay triangulation, as well as Morse-Smale complexes.

Methods based on Voronoi Diagrams and Delaunay Triangulations. Voronoi diagrams [52, 53] and Delaunay triangulations [13] are well-studied structures that produce meshes from sets of points. We refer the reader to survey articles for an in-depth review [3, 2, 43] and algorithms to compute them [16].

Most of the geometry-based cavity detection algorithms are based upon the computation of Voronoi diagrams, Delaunay triangulations, weighted Delaunay triangulations or their close relative, alpha shapes. Voronoi diagram based techniques have been proposed that have a special focus on the analysis and visualization of tunnels [37, 36], and are implemented in tools such as CAVER [45] and MOLE [44]. In particular, Lindow et. al. [37] provide an overview of all accessible areas of the molecule from the filtered Voronoi diagrams of van der Waals spheres. A followup work [36] used similar constructions to detect structures from a molecular dynamics trajectory. Chakravarty et. al [7] uses a grid-based Monte Carlo procedure to position water molecules in combination with Voronoi-based procedure to identify and quantitate empty space within the solvated protein.

Alpha shapes (concepts closely related to alpha complexes) are sub-complexes of the Delaunay triangulation. Alpha shape theory [19, 21] has been used for the detection of protein cavities [20, 33, 34, 50], appearing in tools such as CAST [35, 14], Proshape [31], CAVER [45] and MolAxis [55]. For example, CAST [35] employs alpha shapes and the discrete flow within Delaunay triangulation [21, 15, 17, 18] to identify and measure protein pockets. A related concept similar to Alpha shape is referred to as the *Beta shape* [28]. It is shown to be better in terms of remaining connected for all resolutions. Beta shape has been used to represent the proximity among the atoms on the boundary of a molecule in defining cavities [29].

Methods based on Morse or Morse-Smale Complexes. A few works exist that employ the Morse complex or Morse-Smale complex in shape analysis. The topological spine [12] encodes the spatial relationships of the extrema of a scalar field together with the local volume and nesting structure of the surrounding contours. It is developed based on the extraction of sparse subsets of the Morse-Smale complex and is used as a visual representation that preserves the topological and geometric structure of a scalar field. The work by Cazals et. al. [6] performs Morse-Smale decompositions to the discrete gradient vector field induced by Connolly's function for molecular surface models. Natarajan et. al. [41] decompose the protein surfaces into segmented features based on the Morse theory, identify rigid components of protein molecules and study the role of cavities and protrusions in protein-protein interactions. Both of these works focus on studying

surface geometry of the proteins, while our proposed technique studies both surface and interior structures.

Bajaj et. al. [5] propose a systematic use of the distance function induced by an isosurface to model structural features of molecules, in particular, by computing stable and unstable manifolds of the critical points of such a distance function. Their approach geometrically complements the encoding of the topology by the contour tree, and enables detection and ranking of the complementary structures of the isosurface, i.e. the tunnels and pockets.

The full Morse-Smale complex has been used to study topological features and to construct hierarchical representations of atomic structures on volume data, identifying the atoms and bonds in a C4H4 molecule and orbitals of a hydrogen atom [26]. Günther et al. [23] present a combinatorial algorithm involving the Morse-Smale complex for the automated extraction and characterization of covalent and non-covalent interactions in molecular systems, based on a derived gradient of electron density.

Scalar Field and Diffusion Analysis in Chemistry. In the chemistry literature, relatively little analysis is carried out on the wavefunction field itself, as opposed to atom geometry. Bader analysis [4] decomposes charge density into regions of uniform gradient each associated with one atom, for example using Voronoi partitioning. It is similar to Morse theory in that it uses gradient descent to partition the scalar field, but would not help in identifying tunnels between 1-saddles and minima. Knoll et al. [30] create approximate wavefunction fields for atomistic MD data using radial basis functions averaged from bulk DFT computations; these fields were used for quantifying surface area and volume but not topological analysis. In materials science, analysis of ion diffusion is typically carried out via small-scale DFT computations similar to the ones in our study in Figure 2 (also see, e.g., [56, 1, 42]). Alternately, larger-scale studies are carried out on bulk systems and model diffusion with electric continuum, e.g. with Maxwell's equations [54].

Comparisons to Prior Work. The fundamental difficulty in applying known approaches for analysis of diffusion of lithium in carbon nanospheres is that there are no criteria based on distance, charge density, or any other scalar value to determine which space permits diffusion. In particular, the middle of a blocking ring of carbon may appear the same as a non-blocking ring or even interstitial space in terms of both distance and charge density values. For instance, Lindow et al. [37, 36] determine accessibility by computing channel radii. The work in [5] forms pockets and tunnels by clustering and merging adjacent stable manifolds of critical points based on their scalar value.

Compared to the work in [24], the approach in this paper is much more scalable in extracting and analyzing diffusion paths. The extraction process relies directly on Delaunay triangulation instead of a scalar volume, no extra critical points need to be simplified, and only a partial gradient field is computed. The prior approach would require an excessively large volume to attain the same accuracy, and discretization error of the distance field would create unmanageable numbers of spurious critical points.

4 APPROACH

Problem Statement. Our proposed approach attempts to determine the diffusion characteristics of lithium in a thermally annealed carbon nanosphere. The data output from the molecular dynamics code, which we use as input to our approach, is a set of points A in \mathbb{R}^3 , with each point representing the location of a carbon atom. The model upon which we formulate our approach makes two initial assumptions: first, carbon atoms are bonded if and only if they are closer than 1.8 angstroms; and second, the valence of carbon rings is the primary factor restricting the diffusion of lithium [47].

Many techniques based on Voronoi diagrams and Delaunay triangulation including Alpha and Beta shapes (as reviewed in Section 3) use Euclidean distance metric during computation to detect tunnels in molecules. In contrast, the geometric arrangement of the atoms in the nanosphere (independent of the underlying metric) plays a key role in determining diffusion paths of the diffuser. For instance, the length of the diagonal of a carbon 6-ring may be greater than the distance

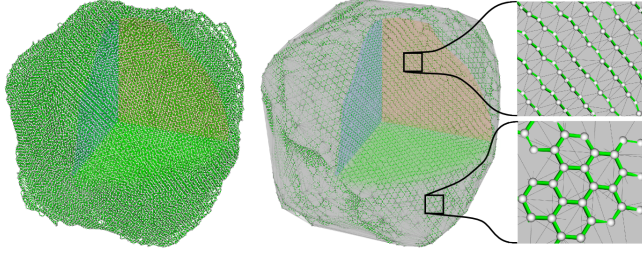


Fig. 4. A carbon nanosphere with 90K atoms (left) is output from a molecular dynamics simulation as a set of atom locations. Carbon atoms (white spheres) closer than 1.9 angstroms are considered bonded (green cylinders). The Delaunay triangulation (gray triangles) of the set of atom positions (right) has carbon atoms at vertices, and a subset of the edges form the bonds. The carbon atoms are generally arranged in concentric graphitic sheets, with the interlayer distances approximately equal to the diagonal length of a carbon 6-ring.

separating two layers of graphitic carbon; lithium is prevented from diffusing across the former, while may move freely in the interstitial space in the latter. Therefore, we are motivated to study the local, geometric arrangements of carbon atoms.

Our proposed approach extracts the free diffusion regions and surfaces within the nanosphere by computing a subcomplex of the Delaunay triangulation. Given a set of points $A \subset \mathbb{R}^3$ that determines carbon atom locations, our computation is rather straightforward. First, we compute the Delaunay triangulation K of A and identify a subset of edges in K that corresponds to *bonds* between atoms; these bonds further define atom *rings* of various valence (and thus size). Second, we apply the *ring-patch* algorithm to compute the sets of triangles that form patches that fill the interior of every ring of bonded atoms; patches for rings with valence d or less are considered as *blocking* patches that prevent lithium diffusion due to their geometry. Finally, we characterize the interstitial spaces within the nanosphere by identifying paths that do not cross blocking patches, therefore extracting the free diffusion regions.

Identifying atoms and bonds. As noted in section 2, the Delaunay triangulation has the representative capacity to encode features of the distance function, and provides a discretization of the space occupied by the nanosphere. We utilize the publicly available software TetGen [49] to construct a Delaunay triangulation K (represented as a simplicial complex) from a set of input points A that corresponds to atom locations. Let A , E , F and T represent the sets of vertices, edges, triangles and tetrahedra in K , respectively. An edge in K is identified as a *bond* between atoms if two of its vertices are closer than a given threshold c . The set of bonds in K is denoted by B . Graphitic carbon has a known covalent bond length of 1.42 Angstroms, however, variability due to thermal energy necessitates a more in-depth analysis, provided in Section 5. In Fig. 4 we show the computed Delaunay triangulation of the set of atom locations, and the corresponding set of extracted atom bonds.

A simple cycle formed by atoms and bonds in K is referred to as an *atom ring*. The *valence* of a ring is its number of atoms. A 2D subcomplex P (i.e. a set of triangles together with its lower-dimensional faces) of K forms a *patch* of a ring R , if the boundary of P is R , i.e., $R = \partial(P)$. Intuitively, a patch closes the hole in the middle of a ring, and it is homotopy equivalent to a 2D disk. As the lithium atom can move in the interstitial space, a *diffusion path* is represented as a sequence of alternating triangles and tetrahedra, starting and ending in tetrahedra, $\{t_0, f_0, \dots, t_i, f_i, t_{i+1}, \dots, t_n\}$, that represents the cells intersected by the path of a moving lithium atom.

4.1 Ring-Patch Algorithm

The input to the ring-patch algorithm, Algorithm 1, is a Delaunay triangulation K where all its vertices are atom locations, a set B of bond edges, and an integer constant d . The output of the algorithm is a set of patches \mathbb{P} for rings of valence d or less.

The algorithm draws inspiration from discrete Morse theory, in

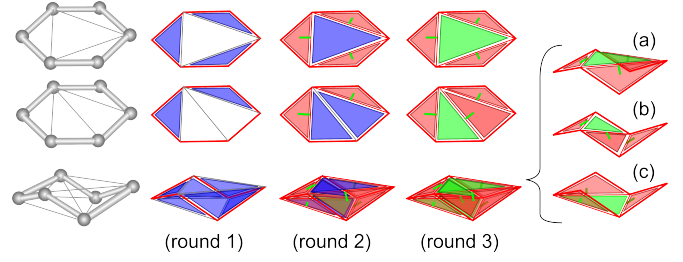


Fig. 5. The progress of Algorithm 1 is displayed for three different triangulations of a valence 6 carbon ring. The top two are planar, while the bottom configuration is more typical in the three-dimensional data. Each round shows the state of the algorithm after line 17; blue indicates triangles that have been enqueued, red or green indicates edges and triangles that have been assigned, with critical triangles marked in green. The top two configurations each yield one patch, while the bottom configuration yields three valid patches (a-c).

Algorithm 1 RingPatch(K, B, d)

```

1: Patches  $\mathbb{P} = \{\}$ 
2:  $V = \{\}$ 
3:  $A = K^0, E = K^1 \setminus K^0, F = K^2 \setminus K^1$ 
4: for  $v \in A$  do:  $V = V \cup \langle v, v \rangle$ ; done
5: for  $e \in B$  do:  $V = V \cup \langle e, e \rangle$ ; done
6: for  $i \in [1, \dots, d]$  do
7:   Queue  $q = \{\}$ 
8:   for  $f \in F$  do: if  $f.\#assignededges() \geq 2$  :  $q.insert(f)$ ; done
9:   while not  $q.empty()$  do
10:     $f = q.top(); q.pop()$ 
11:    if  $f.\#assignededges() = 2$  then
12:       $e = f.unassignededge()$ 
13:       $V = V \cup \langle e, f \rangle$ 
14:    else if  $f.\#assignededges() = 3$  :
15:       $V = V \cup \langle f, f \rangle$ 
16:    endif
17:   end while
18: end for
19: for  $f \in F$  s.t.  $\langle f, f \rangle \in V$  do
20:    $P_f = descendingManifold(f, V)$ 
21:    $R_f = \partial P_f$ 
22:   if  $issimplecycle(R_f)$  and  $\#triangles(P_f) = \#edges(R_f) - 2$  then
23:      $\mathbb{P} = \mathbb{P} \cup P_f$ 
24:   end if
25: end for
26: return  $\mathbb{P}$ 

```

particular, in interpreting discrete vectors as simple homotopy type collapses and expansions. The intermediate state of the algorithm is stored in a partial discrete vector field V . We begin the algorithm with the subcomplex K_0 of K^1 formed by atoms $v \in A$ and bonds $e \in B$, and build a filtration by adding edges and triangles. Each vertex and edge in K_0 is marked critical in V . To grow the filtration, each step of the algorithm adds either a triangle-edge pair to K_i , or if all edges of the triangle are present, then just a single triangle. The $\#assignededges()$ function simply counts the number of edges of a triangle that have been previously assigned. A triangle-edge pair can be added when the two other edges are already in K_i , and the *unassignededge()* function identifies that edge of a triangle. Adding a triangle-edge pair is a simple homotopy type preserving operation, and is recorded by assigning a discrete vector between the cells in V . Adding a single triangle closes a hole, and the topological change is recorded in V by marking it critical.

There may be many candidate triangle-edge pairs or critical triangles to choose from at any given time; we simulate a breadth-first traversal by performing expansions in rounds. In each round, all triangles with two or more assigned edges are entered into the queue.

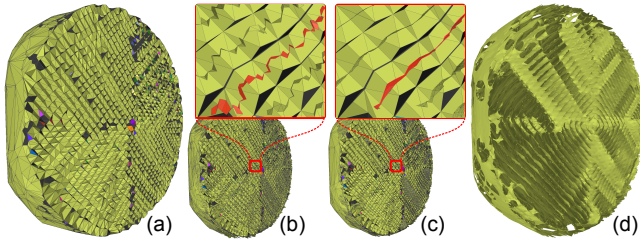


Fig. 6. Triangles of K are colored either dark gray, if they are part of blocking patches, or a random color assigned to each void to which they belong. We generate a dual surface to the volumetric labels (b) by inserting triangles whose corners have the same void label. This surface is smoothed (c) to reveal the large-scale connectivity of the free diffusion surface (d). One layer of the generated surfaces in (b) and (c) are highlighted in red, and show the effect of smoothing.

When a triangle is popped off the queue, its number of unassigned edges is counted, and the triangle is either paired or marked critical. After $\lceil d/2 \rceil$ rounds, the descending manifolds of critical triangles in V are guaranteed to cover all ring patches for rings of valence d or less. However, not all critical cells and their descending manifolds are patches: only those with $\# \text{triangles} = \# \text{edges} - 2$. This restriction prevents degeneracies, such as pouches, from being reported as patches. The *descendingManifold(f, V)* function computes the descending manifold of a critical triangle by adding cells in V -paths through a breadth-first search. The *isSimpleCycle(R_f)* function traverses the vertices and edges in the boundary of a descending manifold to check that it forms a simple cycle. Non-simple cycles indicate degeneracy in a patch, leading to the patch being discarded.

4.2 Computation of Free Diffusion Regions and Surfaces

The ring-patch algorithm returns a set of patches that fill the interior of carbon rings up to a certain valence. We formulate explicitly the two mechanisms of lithium motion illustrated in Fig. 2, namely, ring valence regulating interlayer diffusion, and free interstitial diffusion. We investigate the hypothesis that small defects, i.e., rings of valence 7, 8 and 9, are gatekeepers in lithium diffusion between regions of the carbon nanosphere. We call a region a void when it is completely enclosed by a graphitic shell formed by rings with a maximum valence d . To compute voids and how they are connected to one another explicitly for any given ring valence d , we look at how patches affect lithium diffusion between tetrahedra. We define patches for rings with valence d or less as *blocking patches* that prevent lithium diffusion. We can therefore compute voids as connected volumetric regions, where two tetrahedra are in the same void if and only if there exists a diffusion path between them that does not intersect any blocking patches. We construct a graph whose nodes are tetrahedra, and add an undirected arc between each pair of nodes whose corresponding tetrahedra share a non-blocking triangle in K . A connected component algorithm is used to extract the individual voids. Fig. 6(a) shows the voids as colored regions of the 90K nanosphere, with blocking patches rendered as gray triangles.

The visualization of the voids shown in Fig 6 does not sufficiently show *how* a lithium atom is able to diffuse within uniformly labeled voids. Recognizing that the blocking patches form two-dimensional layers, it is natural to represent the interstitial space itself as a surface. Such a surface can represent the two degrees of freedom of free interstitial lithium motion that are not constrained by the blocking patches.

We construct the surface by examining the labels from the connected component algorithm. For each tetrahedron t_i , for each of its face triangles f_j , and for each of f_j 's edges e_k , we construct the triangle $(C(t_i), C(f_j), C(e_k))$, where $C(\cdot)$ gives the centroid of a simplex, if and only if every tetrahedral co-face of f_j and e_k belongs to the same component as t_i and f_j is not part of any blocking patch. Fig. 6(b) illustrates the surface created from the labeled triangulation. We apply Laplacian smoothing to the resulting surface to improve the visual quality, shown in Fig. 6(c) and (d). The actual paths of diffusing lithium particles would likely exhibit even greater vibrational momen-

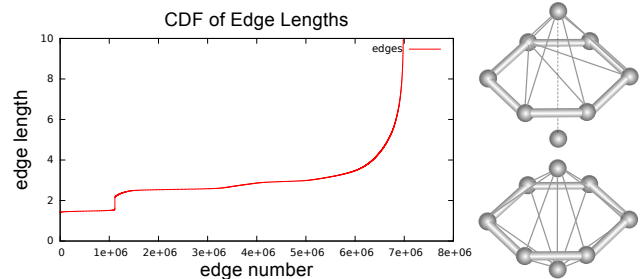


Fig. 7. The jump in the cumulative density function of edge lengths (left) of the Delaunay triangulation shows that bond edges, those with length less than 1.8 Å, are extracted without ambiguities. The technique for computing patches breaks down when the layers are closer together than a bond length (right), in which case the triangulation flips and no set of triangles form a patch of the ring.

tum than we can represent via these surface structures. In our examples, we used 10 iterations of Laplacian smoothing, based solely on user preference for visualization of the result. Though artificial, the smoothing step compensates for the piecewise-linear nature of the Delaunay triangulation, with the goal of better representing average paths of diffusing particles over time. We make an assumption that the initial free surfaces are uniformly crooked, therefore uniform smoothing will have little effect on *relative* geodesic distances along those surfaces.

5 DISCUSSION

A key to our technique is perfect identification of bonds between carbon atoms. Although the expected length in graphene is 1.42 Å, in the result of the MD simulation, the carbon atoms are not in a uniform structure and furthermore thermal energy causes jitter in their positions. However, as shown in Fig. 7, when all edges of the Delaunay triangulation are plotted, there is a clear separation between those edges with length greater than 2.1 Å and those with length less than 1.6 Å. Guided by experiment [47], we used 1.8 Å as the stable distance threshold to determine if two carbon atoms are bonded.

Implicit in our technique is the assumption that the Delaunay triangulation possesses triangles that mesh the interior of a ring. This is equivalent to the statement that there are 2-saddles in the distance function whose descending manifolds close the ring. However, it is possible to have geometric arrangements of atoms that violate these assumptions. For instance, if two carbon atoms are positioned on opposite sides of a ring, in the direction normal to the plane of the ring, then if they are closer together than the diameter of the ring, the triangulation flips, and no disk of triangles closes the ring. This configuration is illustrated in Fig. 7. For sheets of graphene with 6-rings, the diameter is two times the bond length, and therefore the sheets must be at least separated by at least the bond length. In practice, the separation tends to be roughly two times what is needed to guarantee the presence of 2-saddles in the distance function.

The model determining lithium diffusion through carbon rings assumes planar morphology. In practical applications, it is rare for the rings to be truly planar, and instead, the atoms are typically displaced in the third dimension by a small amount, as illustrated in Fig. 5(bottom). In such cases, there is no unique patch closing the ring; several patches close the ring, trapping a volumetric region between them. These slivers make up 0.2% of the volume of the nanosphere. In practice, they do not affect the overall diffusion properties, as all patches for the same ring behave in similar manner, as only valence of the ring is taken into consideration.

Implementation. The simplicial complex used as the input mesh was generated with TetGen [49]. The approach in Section 4 was implemented in c++ and run on a single core of a shared memory machine, taking approximately 5 minutes to perform the full analysis, generating annotated meshes and surfaces. The majority of time was spent in reading and constructing the simplicial complex, and writing surfaces in formats supported by downstream visualization tools. Subsequent visualizations were produced using MeshLab [9] and VisIt [8].

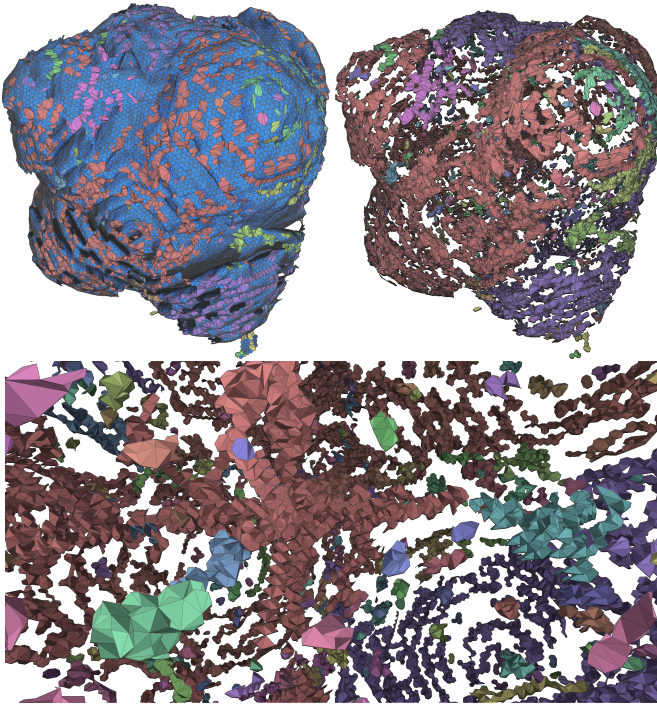


Fig. 8. The patches of rings with valence six or less are shown in blue (top left) for the 740K nanosphere. The other colors are patches for small defects, rings up to valence 10. These are clustered near the exterior (top right) or along the principle axes (bottom) in the interior of the sphere. Defect patches with the same color touch along at least one atom of their rings, and the large components indicate that defect rings occur in the neighborhood of other defects.

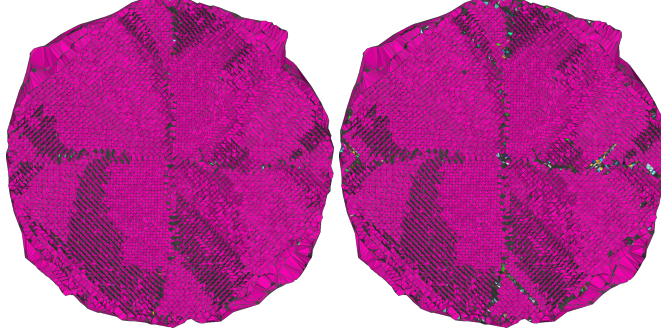


Fig. 9. We show the voids of the 740K nanosphere for two different thresholds of valence that marks rings as blocking or not. On the left, any ring with valence greater than six permits free diffusion of lithium. On the right, any ring with valence ≤ 12 blocks flow. In both images, the dark pink region is the largest void, connected to the exterior. Surprisingly, the two void images are almost identical, with some minor differences. This suggests that small-scale defects are not the primary mechanism of interlayer lithium diffusion.

6 RESULTS

Experimental results were generated for both a 90K and 740K atom simulations, showing similar characteristics. We focus on the 740K simulation in this section as it more closely approximates real-world nanosphere sizes.

Defects The traditional atom-and-bond visualization of 740K nanosphere is shown in the teaser image. It is challenging to identify any patterns of defects in the traditional image, and therefore in Fig. 8 we present a visualization of all blocking and non-blocking patches extracted by our approach. It becomes apparent that small defects occur with highest concentrations near the surface of the nanosphere, or along the principle axis leading to the center. Indeed, the interiors of the eight regions bounded by the $x = 0$, $y = 0$, and $z = 0$ planes and

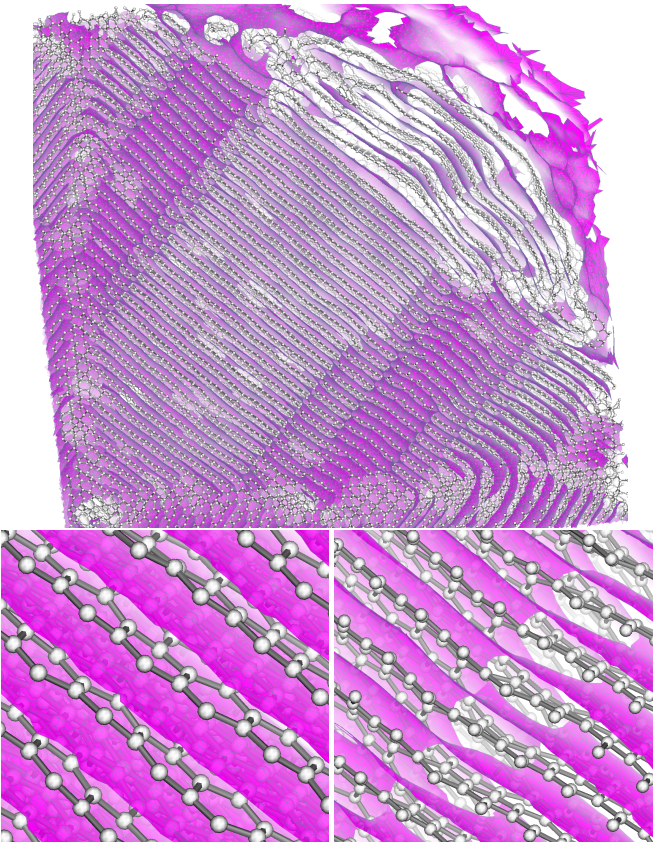


Fig. 10. Uniformly labeled voids from Fig. 9 are converted to free diffusion surfaces (pink surfaces), and rendered with the atoms (gray spheres) and bonds (gray cylinders) for the 740K nanosphere (top). While small-scale defects contribute to lithium diffusion, the free surfaces highlight a more pervasive mechanism: large scale dislocations propagating through graphitic layers. Defect-free graphitic layers (bottom left) are broken along coherent dislocations (bottom right), which connect the free diffusion surface of different layers.

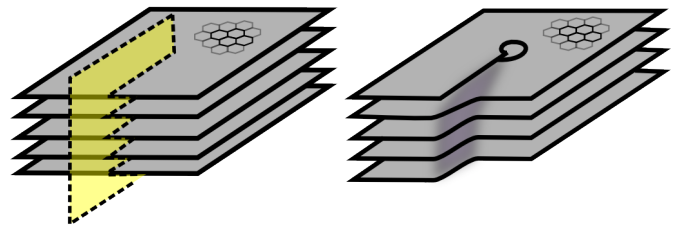


Fig. 11. We propose a model for the creation of defects in the nanosphere, namely the propagation a fault (left), dislocation, and subsequent reconnection (right) of layers.

nanosphere surface are relatively devoid of defects. Incidentally, the regions with high number of defects correlate to exactly those areas where the stacked graphitic carbon layers bend.

Voids We next investigate the voids in the interior of the carbon nanosphere, and how they are affected by defects. Our initial hypothesis held that the interior of the nanosphere was composed of distinct voids, connected to one another by defects with relatively small valence, e.g. 7-12. Fig. 9 shows our first surprising result, namely that the vast majority of the nanosphere, 97.8% of the volume, is composed of a single void. This behavior does not change, whether only rings with valence less than 7, or those with valence 12 or less are considered blocking for the purposes of delimiting voids. This clearly contradicts our initial hypothesis, suggesting instead that some factor other than defect rings drives lithium diffusion in the nanosphere.

Free Diffusion Surfaces To better understand the mechanics of lithium diffusion, we compute and visualize the free diffusion surfaces. Fig. 10 provides the first insight into the nature of large-scale

defects in the nanosphere. For the first time, we can show that the two-dimensional free diffusion surfaces wrap around their one-dimensional boundary in a helical structure, as illustrated in Fig. 13(b). This structure enables lithium motion in the third dimension, similar to how a spiral staircase allows locally two-dimensional travel to transport between levels. Furthermore, the coherent, linear location of these dislocations suggests a formative process wherein layered graphite is broken and reconnected along faults, as in Fig. 11.

Distance The utility of a material as an anode in a battery is highly dependent on the time needed to saturate the material with lithium ions. Absent the capability to simulate this diffusion, we instead turn to a proxy, namely the minimum distance an ion would have to travel from the interior to the exterior of the nanosphere. The motivation is the hypothetical scenario where lithium ions initially surround a vacant nanosphere, and over time diffuse into the sphere. Recall that the free diffusion surfaces record the approximate mean location of lithium bouncing between layers of graphitic carbon. Therefore, with the assumption that the leading edge of the diffusion progresses at a steady rate, the geodesic distance along free surfaces is a reasonable approximation to the solution.

We consider a triangle of the Delaunay triangulation as exterior if it is either a non-patch boundary triangle, or a face of a tet with an edge longer than 6.8 Å. We utilize the free diffusion surfaces and compute geodesic distance to the exterior. Fig. 12 shows a cross-section of the nanosphere colored by geodesic distance, illustrating that diffusion to the interior is facilitated by dislocations. Furthermore, we can compute how much of the nanosphere is accessible within any distance of the exterior. While small defects did not affect the connectivity of voids inside the nanosphere, we observe a small impact on the rate of diffusion. Namely, we compare the volume vs. distance curves of configurations where rings with valence less than d block the diffusion of lithium. Higher valence rings blocking diffusion results in longer diffusion distance to achieve the same volume of saturation. Finally, in Fig. 13, we extract the boundary curves of the free diffusion surfaces, and provide an illustrative visualization of the regions of the nanosphere accessible at varying distances. These images provide strong support for a new hypothesis that dislocations extending to the surface of the nanosphere are the primary mechanism controlling the rate of saturation in carbon nanospheres.

7 CONCLUSION/FUTURE WORK

We have presented a new approach for studying lithium diffusion characteristics in carbon nanospheres used as battery anode materials. We showed, for the first time, that the majority of the interior of the nanosphere was directly accessible to its exterior via major dislocations. The visualizations of the free diffusion surfaces further led to a hypothesis for the formation of these dislocations, which will be tested in future experiments. We finally quantified the contribution of small-scale defects to the overall accessible volume, and furthermore their effect on the speed of saturation.

The major finding of this work is that local defects, rings with high valence, have relatively insignificant contribution to the adsorption characteristics of this carbon nanosphere. We anticipate that this study will enable the systematic analysis of nanospheres computed in different configurations to be able to quantify the effects of changing geometries and physical processes. This could lead to rethinking how best to create nanospheres to have desirable cycling properties in batteries.

We will extend this work to study large scale amorphous mesoporous carbon structures, a 3D periodic repeated structure. An additional target will be studying carbon nanosphere matrices, where each sphere is bonded with others to form a periodic matrix. We plan on extending the technique to handle multi-material MD computations, for instance, to study the effect of dopants or coating layers. Use of this analysis at simulation checkpoints could be useful for computational steering, to terminate unpromising simulations where diffusion cavities are unlikely to develop. Our technique should also be applicable to other silicon-based anode materials, and extended to larger, experimental-scale nanospheres. In addition, we will use the extracted

geometries to accelerate more accurate “dynamics-like” analysis to compute adsorption rates.

ACKNOWLEDGMENTS

This research was supported as part of the Center for Electrical Energy Storage (CEES), an Energy Frontier Research Center (EFRC) and Argonne Leadership Computing Facility under the U.S. Department of Energy, Office of Science, Office of Basic Energy (Award Number DE-AC02-06CH11357). This work was also supported in part by the NSF CISE ACI-0904631 at the University of Utah. We would like to thank Mark West and Intel Corporation for their generous donation of hardware.

REFERENCES

- [1] R. Ali, M. Yashima, Y. Matsushita, H. Yoshioka, K. Ohoyama, and F. Izumi. Diffusion path of oxide ions in an apatite-type ionic conductor la9. 69 (si5. 70mg0. 30) o26. 24. *Chemistry of Materials*, 20(16):5203–5208, 2008.
- [2] F. Aurenhammer. Power diagrams: properties, algorithms and applications. *SIAM J. Comput.*, 16:78–96, 1987.
- [3] F. Aurenhammer. Voronoi diagrams – a study of a fundamental geometric data structure. *ACM Comput. Surveys*, 23:345–405, 1991.
- [4] R. F. Bader. *Atoms in molecules*. Wiley Online Library, 1990.
- [5] C. Bajaj, A. Gillette, and S. Goswami. Topology based selection and curation of level sets. In H.-C. Hege, K. Polthier, and G. Scheuermann, editors, *Topology-Based Methods in Visualization II, Mathematics and Visualization*, pages 45–58. Springer Berlin Heidelberg, 2009.
- [6] F. Cazals, F. Chazal, and T. Lewiner. Molecular shape analysis based upon the morse-smale complex and the connolly function. *Proceedings 19th Annual Symposium on Computational Geometry*, pages 351–360, 2003.
- [7] S. Chakravarty, A. Bhinge, and R. Varadarajan. A procedure for detection and quantitation of cavity volumes in proteins. *Journal of Biological Chemistry*, 277(35):31345–31353, 2002.
- [8] H. Childs, E. Brugger, K. Bonnell, J. Meredith, M. Miller, B. Whitlock, and N. Max. A contract based system for large data visualization. In *Visualization, 2005. VIS 05. IEEE*, pages 191–198. IEEE, 2005.
- [9] P. Cignoni, M. Corsini, and G. Ranzuglia. Meshlab: an open-source 3d mesh processing system. *Ercim news*, 73:45–46, 2008.
- [10] A. J. Cohen, P. Mori-Sánchez, and W. Yang. Challenges for density functional theory. *Chemical Reviews*, 112(1):289–320, 2011.
- [11] M. M. Cohen. *A course in simple-homotopy theory*. Graduate Texts in Mathematics. Springer, New York, 1973.
- [12] C. D. Correia, P. Lindstrom, and P.-T. Bremer. Topological spines: A structure-preserving visual representation of scalar fields. *IEEE Transactions on Visualization and Computer Graphics*, 17(12):1842–1851, 2011.
- [13] B. Delaunay. Sur la sphère vide. *Izv. Akad. Nauk SSSR, Otdelenie Matematicheskii i Estestvennyka Nauk*, 7:793–800, 1934.
- [14] J. Dundas, Z. Ouyang, J. Tseng, A. Binkowski, Y. Turpaz, and J. Liang. CASTp: computed atlas of surface topography of proteins with structural and topographical mapping of functionally annotated residues. *Nucleic acids research*, 34(2):W116–W118, 2006.
- [15] H. Edelsbrunner. The union of balls and its dual shape. *Discrete and Computational Geometry*, 13:415–440, 1995.
- [16] H. Edelsbrunner. *Geometry and Topology for Mesh Generation*. Cambridge Univ. Press, Cambridge, England, 2001.
- [17] H. Edelsbrunner, M. Facello, P. Fu, and J. Liang. Measuring proteins and voids in proteins. In *Proceedings 28th Annual Hawaii International Conference on Systems Science*, pages 256–264, 1995.
- [18] H. Edelsbrunner, M. Facello, and J. Liang. On the definition and the construction of pockets in macromolecules. *Discrete Applied Mathematics*, 88:83–102, 1998.
- [19] H. Edelsbrunner and P. Fu. Measuring space filling diagrams and voids. Technical Report UIUC-BI-MB-94-01, University of Illinois at Urbana-Champaign, 1994.
- [20] H. Edelsbrunner and P. Koehl. The geometry of biomolecular solvation. *Combinatorial & Computational Geometry*, 52:243–275, 2005.
- [21] H. Edelsbrunner and E. P. Mücke. Three-dimensional alpha shapes. *ACM Trans. Graphics*, 13(43–72), 1994.
- [22] R. Forman. A user’s guide to discrete Morse theory. In *Séminaire Lotharingien de Combinatoire*, volume 48, 2002.

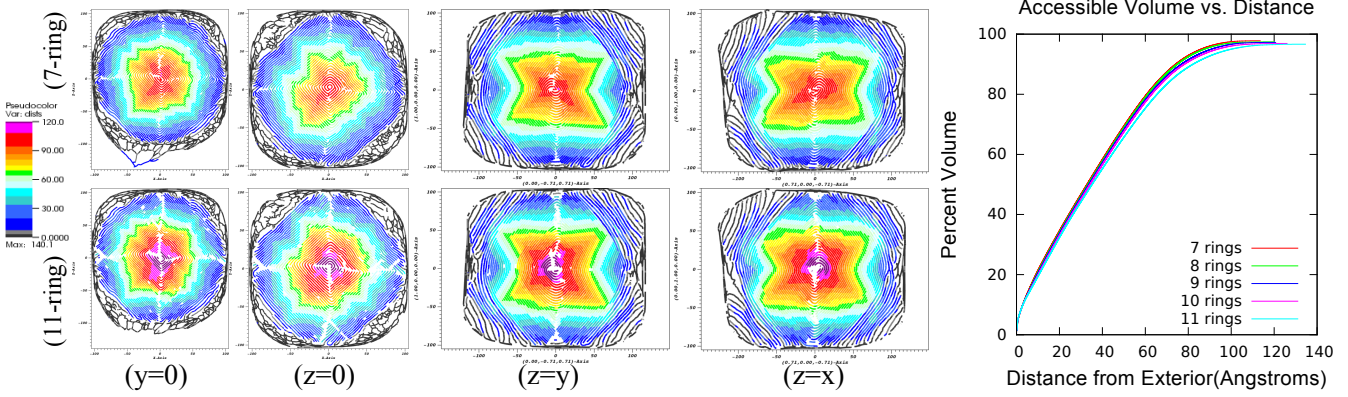


Fig. 12. We show slices through the free diffusion surfaces, oriented along planes slicing through the center of the nanosphere. The top row shows the distances when valence 7 and greater rings permit the free diffusion of lithium. The bottom row show distances when valence 11 or lower rings completely block lithium diffusion. Although in practice any ring with valence greater than 6 permits lithium diffusion, by artificially increasing this number we can investigate the effects of removing small valence defects. The plot on the right shows the percent of the volume that is accessible as a function of distance from the exterior, where each curve represents certain valence rings and above permitting free diffusion. Notably, there is minuscule difference between curves for different valences, implying that small scale defects have only a secondary effect.

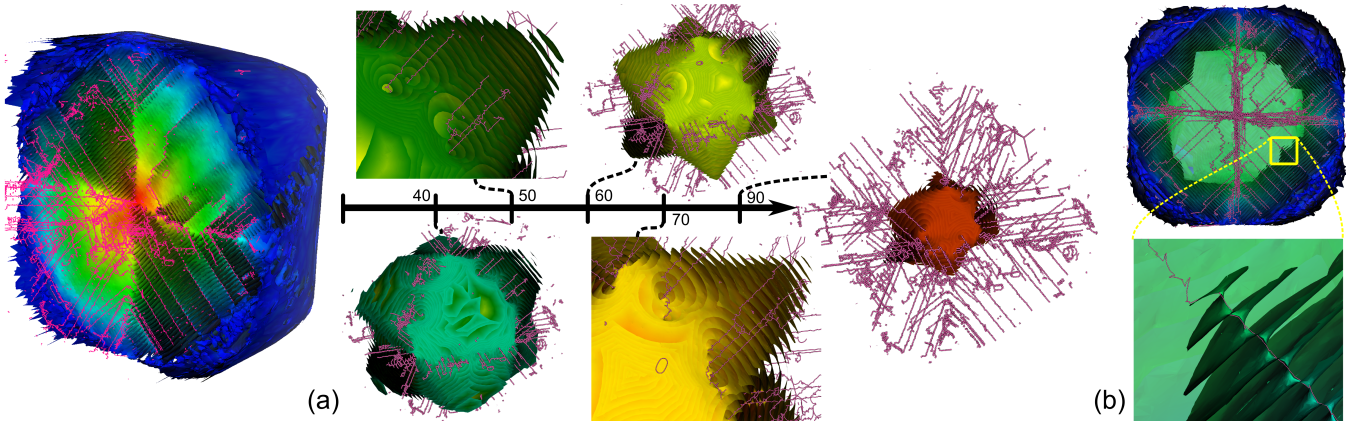


Fig. 13. The boundaries of the free diffusion surfaces are displayed as lines (pink), and the surface is colored according to diffusion distance from the exterior (blue is low, red high). The surface above a distance threshold is shown for varying thresholds (a). The boundaries clearly correlate to faster paths into the interior of the nanosphere in the shape of a cone. Protruding cones of layered surfaces noticeably lack these large scale dislocation features. An alternate view, removing the high distance surface components (b), highlights the efficacy of large scale spiral faults in reducing diffusion distance to the interior of the nanosphere, and simulates the portion of the sphere saturated by lithium for a fixed time.

- [23] D. Günther, R. A. Boto, J. Contreras-Garcia, J.-P. Piquemal, and J. Tierny. Characterizing molecular interactions in chemical systems. *IEEE Transactions on Visualization and Computer Graphics (Proceedings Scientific Visualization 2014)*, 20(12):2476–2485, December 2014.
- [24] A. Gyulassy, A. Knoll, P.-T. Bremer, B. Wang, K. C. Lau, M. E. Papka, V. Pascucci, and L. Curtiss. Morse-Smale analysis of ion diffusion for dft battery materials simulations. *Topology-Based Methods in Visualization (TopoInVis)*, page to appear, 2015.
- [25] A. Gyulassy, A. Knoll, K. C. Lau, B. Wang, P.-T. Bremer, M. E. Papka, V. Pascucci, and L. Curtiss. Morse-smale analysis of ion diffusion in *ab initio* battery materials simulations. In *TopoInVis*, 2015 (to appear).
- [26] A. Gyulassy, V. Natarajan, V. Pascucci, P.-T. Bremer, and B. Hamann. Topology-based simplification for feature extraction from 3D scalar fields. In *Proceedings of the IEEE Visualization 2005 (VIS'05)*, pages 535–542. IEEE Computer Society, 2005.
- [27] N. G. Hörmann, M. Jäckle, F. Gossenberger, T. Roman, K. Forster-Tonigold, M. Naderian, S. Sakong, and A. Groß. Some challenges in the first-principles modeling of structures and processes in electrochemical energy storage and transfer. *Journal of Power Sources*, 275:531–538, 2015.
- [28] D.-S. Kim, Y. Cho, K. Sugihara, J. Ryu, and D. Kim. Three-dimensional beta-shapes and beta-complexes via quasi-triangulation. *Computer-Aided Design*, 42(10):911–929, 2010.
- [29] D.-S. Kim and K. Sugihara. Tunnels and voids in molecules via voronoi diagram. *Proc. Symp. Voronoi Diagrams in Science and Engineering (ISVD)*, pages 138–143, 2012.
- [30] A. Knoll, B. Liu, K. C. Lau, M. K. Chan, A. Sumer, J. Greeley, L. Curtiss, J. Jellinek, M. Hereld, and M. E. Papka. Uncertainty classification and visualization of molecular interfaces. *Intl J. Uncertainty Quantification*, 3(2):157–169, 2013.
- [31] P. Koehl, M. Levitt, and H. Edelsbrunner. Proshape: understanding the shape of protein structures. *Software at biogeometry*, 2004.
- [32] G. Kresse and J. Furthmüller. Efficiency of ab-initio total energy calculations for metals and semiconductors using a plane-wave basis set. *Computational Materials Science*, 6(1):15–50, 1996.
- [33] J. Liang, H. Edelsbrunner, P. Fu, S.-H. P., and S. Subramaniam. Analytical shape computation of macromolecules: II. inaccessible cavities in proteins. *Proteins Structure Function and Genetics*, 33(1):18–29, 1998.
- [34] J. Liang, H. Edelsbrunner, and C. Woodward. Anatomy of protein pockets and cavities. *Protein Science*, 7(9):1884–1897, 1998.
- [35] J. Liang, H. Edelsbrunner, and C. Woodward. Anatomy of protein pockets and cavities: measurement of binding site geometry and implications for ligand design. *Protein Sci.*, 7:18841897, 1998.
- [36] N. Lindow, D. Baum, A. Bondar, and H. Hege. Dynamic channels in biomolecular systems: Path analysis and visualization. *Proc. IEEE Symposium on Biological Data Visualization (BioVis)*, pages 99–106, 2012.

- [37] N. Lindow, D. Baum, and H. Hege. Voronoi-based extraction and visualization of molecular paths. *IEEE Transactions on Visualization and Computer Graphics*, 17(12):2025–2034, 2011.
- [38] P. V. Medeiros, F. de Brito Mota, A. J. Mascarenhas, and C. M. de Castilho. Adsorption of monovalent metal atoms on graphene: a theoretical approach. *Nanotechnology*, 21(11):115701, 2010.
- [39] V. Meunier, J. Kephart, C. Roland, and J. Bernholc. Ab initio investigations of lithium diffusion in carbon nanotube systems. *Physical review letters*, 88(7):075506, 2002.
- [40] J. R. Munkres. *Elements of algebraic topology*. Addison-Wesley, Redwood City, CA, USA, 1984.
- [41] V. Natarajan, Y. Wang, P.-T. Bremer, V. Pascucci, and B. Hamann. Segmenting molecular surfaces. *Computer Aided Geometric Design*, 23(6):495–509, 2006.
- [42] S.-i. Nishimura, G. Kobayashi, K. Ohoyama, R. Kanno, M. Yashima, and A. Yamada. Experimental visualization of lithium diffusion in lixfepo4. *Nature materials*, 7(9):707–711, 2008.
- [43] A. Okabe, B. Boots, K. Sugihara, and S. N. Chiu. *Spatial tessellations: Concepts and applications of Voronoi diagrams*. Wiley, NYC, NY, 2000.
- [44] M. Petřek, P. Košinová, J. Koča, and M. Otyepka. MOLE: A voronoi diagram-based explorer of molecular channels, pores, and tunnels. *Structure*, 15(11):1357–1363, 2007.
- [45] M. Petřek, M. Otyepka, P. Banáš, P. Košinová, J. Koča, and J. Damborský. CAVER: a new tool to explore routes from protein clefts, pockets and cavities. *BMC Bioinformatics*, 7:316, 2006.
- [46] S. Plimpton. Fast parallel algorithms for short-range molecular dynamics. *Journal of computational physics*, 117(1):1–19, 1995.
- [47] V. G. Pol, J. Wen, K. C. Lau, S. Callear, D. T. Bowron, C.-K. Lin, S. A. Deshmukh, S. Sankaranarayanan, L. A. Curtiss, W. I. David, et al. Probing the evolution and morphology of hard carbon spheres. *Carbon*, 68:104–111, 2014.
- [48] H. Shimoda, B. Gao, X. Tang, A. Kleinhammes, L. Fleming, Y. Wu, and O. Zhou. Lithium intercalation into opened single-wall carbon nanotubes: storage capacity and electronic properties. *Physical review letters*, 88(1):015502, 2001.
- [49] H. Si. Tetgen, a delaunay-based quality tetrahedral mesh generator. *ACM Transactions on Mathematical Software (TOMS)*, 41(2):11, 2015.
- [50] R. Sridharamurthy, H. Doraiswamy, S. Patel, R. Varadarajan, and V. Natarajan. Extraction of robust voids and pockets in proteins. *Eurographics Conference on Visualization (short paper)*, 2013.
- [51] J.-M. Tarascon and M. Armand. Issues and challenges facing rechargeable lithium batteries. *Nature*, 414(6861):359–367, 2001.
- [52] G. Voronoi. Nouvelles applications des paramètres continus à la théorie des formes quadratiques. première mémoire: Sur quelques propriétés des formes quadratiques positives parfaites. *J. Reine Angew. Math.*, 133:97–178, 1907.
- [53] G. Voronoi. Nouvelles applications des paramètres continus à la théorie des formes quadratiques. deuxième mémoire: Recherches sur les parallélédres primitifs. *J. Reine Angew. Math.*, 134:198–287, 1908.
- [54] X. Wang, B. Shapiro, and E. Smela. Visualizing ion currents in conjugated polymers. *Advanced Materials*, 16(18):1605–1609, 2004.
- [55] E. Yaffe, D. Fishelovitch, H. J. Wolfson, D. Halperin, and R. Nussinov. Molaxis: efficient and accurate identification of channels in macromolecules. *Proteins*, 73:72–86, 2008.
- [56] M. Yashima, M. Itoh, Y. Inaguma, and Y. Morii. Crystal structure and diffusion path in the fast lithium-ion conductor la_{0.62}li_{0.16}ti_{0.3}. *Journal of the American Chemical Society*, 127(10):3491–3495, 2005.